Proceedings of the Canadian Society for Mechanical Engineering International Congress
32nd Annual Conference of the Computational Fluid Dynamics Society of Canada
Canadian Society of Rheology Symposium
CSME-CFDSC-CSR 2025
May 25–28, 2025, Montréal, Québec, Canada

Numerical analysis of heat-generating terms in the energy equation for wire arc additive manufacturing

E. Asgari[1], M. Saeedi[1], J. Nafar Dastgerdi[2], A. Nasiri[1*]
[1]Department of Mechanical Engineering, Dalhousie University, 1360 Barrington St., Halifax, NS B3H 4R2, Canada
[2]Mechanical Engineering Group, School of Engineering, University of Kent, Canterbury, CT2 7NT, United Kingdom
*Ali Nasiri: ali.nasiri@dal.ca

Abstract— Wire Arc Additive Manufacturing (WAAM) primarily utilizes Gas Metal Arc (GMA) as its heat source, yet discrepancies in the thermal modeling of the process persist in the literature. This study presents a computational fluid dynamic (CFD)-based numerical investigation of heat distribution in a typical GMA process used in WAAM, focusing on the influence of boundary conditions, initial values, and source terms in the energy equation. The findings highlight the critical role of initial electric potential and temperature in determining the steady-state thermal profile. Additionally, the significance of the electric-migration generation term is demonstrated, which cannot be neglected. These insights contribute to improving the accuracy of computational simulations for WAAM, aiding future research in refining process modeling and optimization.

Keywords: CFD; WAAM; GMA; Thermal modelling; Temperature distribution

I. Introduction

This paper investigates the numerical configuration of a test case for a GMA heat source, commonly employed in WAAM [1], within a CFD framework. While GMA-WAAM technology is widely employed as an additive manufacturing technique, limited studies focus on its CFD simulation. Additionally, there are some ambiguities regarding the numerical approach and boundary conditions.

Lowke et al. [2] developed a model for calculating heat, potential, and electromagnetic forces in a free-burning arc column, which later served as a basis for future numerical studies. Several researchers have refined this model with various modifications [3–8]. In addition to this approach, a more simplified method has been employed to model the effects of electromagnetic forces and heat sources on the fluid flow transport equations [9–14]. However, this simplified approach relies on additional constants and input parameters, potentially reducing its practicality. Conversely, the first approach utilizes Maxwell's equations to calculate electric potential and current density. However, it is computationally more demanding as it requires solving three additional transport equations (in a 3-D domain) to account for electric potential and magnetic field components.

In the current study, we adopt the first approach mentioned earlier, i.e. the one incorporating Maxwell's equations, focusing on thermal modelling and the associated source terms that play a crucial role in molten droplet dynamics. We aim to clarify ambiguities in previous numerical studies and evaluate the impacts of initial conditions and electric potential boundary flux on the final outcome of numerical modeling.

II. Numerical Setup

A. Computational Domain

The computational domain is illustrated in Figure 1, with boundary types indicated. The simulation domain is adopted from the work presented in [5], considering an axisymmetric configuration for reducing complexity. However, the internal domain within the wire (Anode) is omitted for simplicity, as implemented in recent studies [3,4]. A total number of 9000 cells were generated using GridPro [15] that minimizes skewness and provides a high-quality structured mesh.

B. Governing Equations

The governing equations for the GMA droplet dynamics are the continuity, momentum, and energy equations, as well as the volume of fluid (VOF) equation for interface tracking and Maxwell's equations for calculating the electric potential and current density, which follow as:

$$\frac{\partial \rho}{\partial t} + \nabla.(\rho v) = 0 \tag{1}$$

$$\frac{\partial (\rho v)}{\partial t} + \nabla.(\rho v v) = -\nabla P + \nabla.\tau + S_m \tag{2}$$

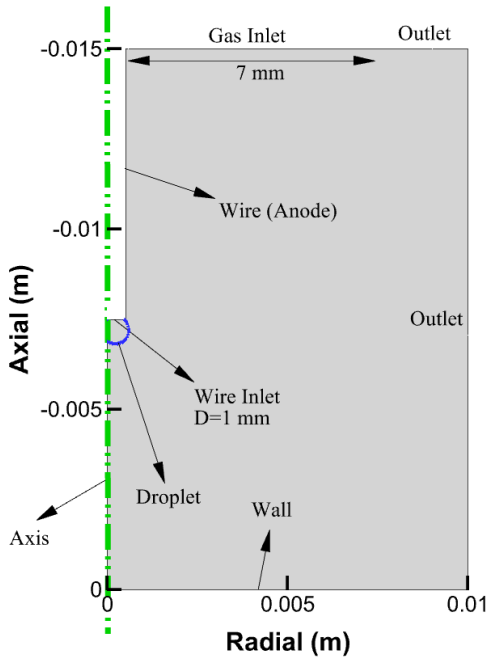

Figure 1. The adopted computational domain with boundary types.

$$\frac{\partial(\rho H)}{\partial t} + \nabla.(\rho v H) = \nabla.(k\nabla T) + S_e \tag{3}$$

$$\frac{\partial F}{\partial t} + (v.\nabla)F = 0 \tag{4}$$

In the equations above, ρ, v, P, and T refer to the fluid density, velocity, pressure, and temperature, respectively. τ represents the flow shear stress tensor and F denotes the volume of fluid fraction (ranging from 0 to 1). However, as mentioned in the Introduction, this study focuses solely on heat transfer and the Maxwell-Poisson equation for electric potential, as follows:

$$\nabla.(\sigma\nabla\varphi) = 0 \tag{5}$$

$$J = -\sigma\nabla\varphi, \tag{6}$$

where φ refers to the electric potential, σ represents the electrical conductivity and J denotes the current density vector. In Eq. (3), the source term S_e consists of two terms, as described by [2]:

$$S_e = \frac{|J|^2}{\sigma} - U, \tag{7}$$

where the first term refers to Joule-heat, and U stands for the emission cooling rate, which is a function of the net emission coefficient. However, more recent studies have included additional terms for the anode-plasma interface:

$$S_e = \frac{|J|^2}{\sigma} - U + |J|\omega - \varepsilon\sigma_{SB}T^4\,, \tag{8}$$

where σ_{SB}, ω, and ε refer to the Stefan-Boltzmann constant, work function, and emissivity of the wire anode, respectively. However, more recent studies have introduced an additional term to account for electron migration: $\frac{5k_b}{2e}(J.\nabla T)$ [3,7,16]. There are some inconsistencies in the literature regarding the inclusion of source terms. For example, [4] omitted the electron migration term but included the anode-plasma interface in Eq. (8), multiplied by $|\nabla F|$, which can significantly increase the value of fine meshes. In contrast, [3] did not consider this term at all. In the current study, we consider all source terms in the energy equation and apply the anode-plasma term only to the interfacial cells.

As seen in Eq. (4) through Eq. (8), there is a strong coupling between the energy equation and Maxwell's equations due to the presence of source terms in the former. In fact, the source terms arising from Maxwell's equations are responsible for the temperature distribution in the plasma region. To investigate this coupling, we use a volume fraction field obtained from an initial solution without the heat sources and only solve for the momentum, energy, and electric potential. A similar technique was previously used in [4] to stabilize the plasma temperature before adding the momentum source terms. Also, [3] demonstrated that the overall temperature distribution in the plasma region remains unchanged when the droplet develops and detaches from the wire. We exploit this observation to investigate the terms of energy source and electric potential boundary conditions. With regard to the latter, [2] used a uniform current density at the wire inlet to specify a Neumann boundary condition for the electric potential. Later, other studies [3–5,7,17] extended this assumption and applied a simple relation for the current density at the inlet: $J_0 = \frac{I}{\pi r_w^2}$, where I refers to the welding current and r_w represents the wire radius. Therefore, the following relation is applied to the wire inlet as the electric potential boundary condition.

$$-\sigma\frac{\partial\varphi}{\partial y} = \frac{I}{\pi r_w^2}, \tag{9}$$

where y refers to the axial direction. As for the electrical conductivity σ, it should be noted that it is a field quantity rather than a constant value, depending on the medium, whether plasma or metal. [2] stated that metal electrical conductivity should be used for the above boundary condition. We will investigate the impact of this parameter on the temperature field. However, there is one issue with eq. (9): the current density vector should be heading downward through the wire anode. Therefore, a negative sign should also be included on the right-hand side of eq. (9). Unfortunately, the literature has shown inconsistencies and ambiguities in this regard. For example, [3] has not included σ in their formulation, [16] has implemented a Dirichlet condition instead of a Neumann type, or [18] specified a zero-gradient (zero current) boundary condition in their study.

Therefore, it is necessary to clarify the effect of the boundary flux on the temperature distribution. In addition, we will examine the significance of each source term in the energy equation to determine their relative importance.

For the simulations, we have considered the parameters and feedstock material introduced in [5]. Argon shielding gas was set to a flow rate of 10 L/min, and the WAAM current was fixed at 350 A. The wire anode is made of normal carbon steel with an electrical conductivity of 7.7e+5 S/m, and the inlet temperature was set to 2000K. For the outlet surfaces, a Neumann condition was assigned to the temperature, and a fixed value, as specified in [5], was used for the wire and bottom surfaces. The electric potential boundary condition at the ground ($y = 0$) was specified as zero, and a Neumann boundary condition was assigned to the outlet and wire surface boundaries.

III. Results

Figure 2 presents temperature distribution resulting from an initial temperature of 300K and an electric potential of 0V. The white dashed line represents the droplet boundary. It is seen that the plasma gas temperature is primarily influenced by the boundary conditions, including those at the wire tip and the bottom wall. Figure 3 shows the temperature distribution obtained with an initial temperature of 15,000K assigned to the region between the wire tip and the bottom. Noteworthy, the initial electric potential was set to 11V. It was found that assigning both initial temperature and potential is required to achieve a realistic temperature distribution that closely matches the results in [5].

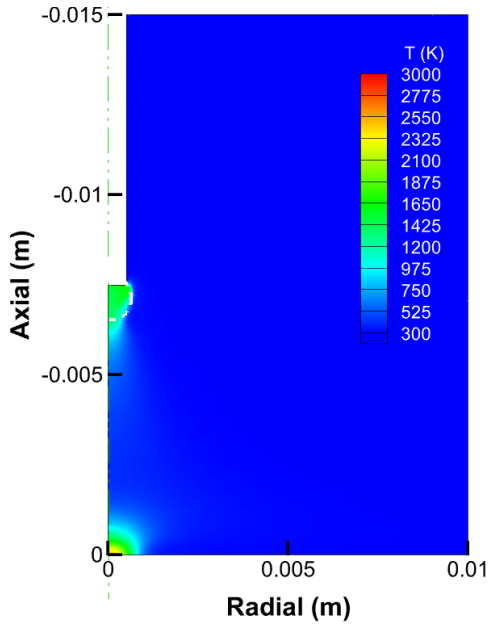

Figure 2. Temperature distribution with T_{init}=300K.

To investigate the effect of electric potential boundary flux, two additional values are examined, and the resulting temperature distributions are presented in Figure 4 and Figure 5.

It should be noted that the original boundary flux in eq. (9) was 580 in the previous plots. The results show that the overall temperature distribution is not significantly affected by the boundary flux, with only minor variations near the droplet. This finding may justify the inconsistencies in the literature regarding the boundary flux value, as highlighted in the previous section, and conveys the larger dependence of temperature on the material properties, i.e. the electrical conductivity.

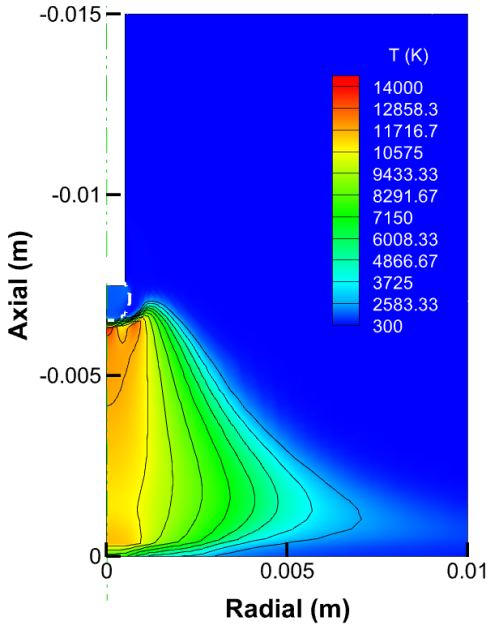

Figure 3. Temperature distribution with T_{init}=15000K.

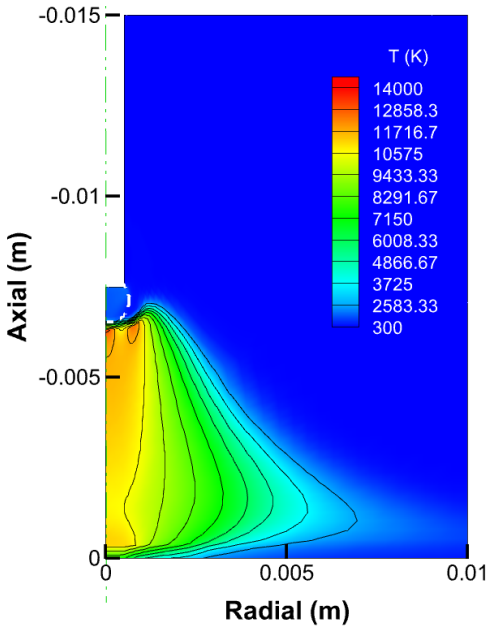

Figure 4. Temperature distribution with $\frac{\partial \varphi}{\partial y} = 2400$.

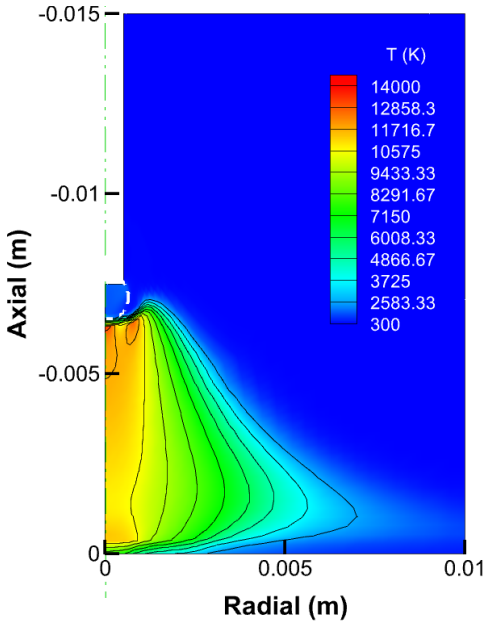

Figure 5. Temperature distribution with $\frac{\partial \varphi}{\partial y} = 10000$.

As explained in the section "Numerical Setup", there are four source terms in the energy equation that influence the temperature distribution. It was mentioned that some studies omitted one or two of these terms in their calculations. In this study, it was aimed to identify the contribution of each of these source terms to clarify their impact on the temperature field.

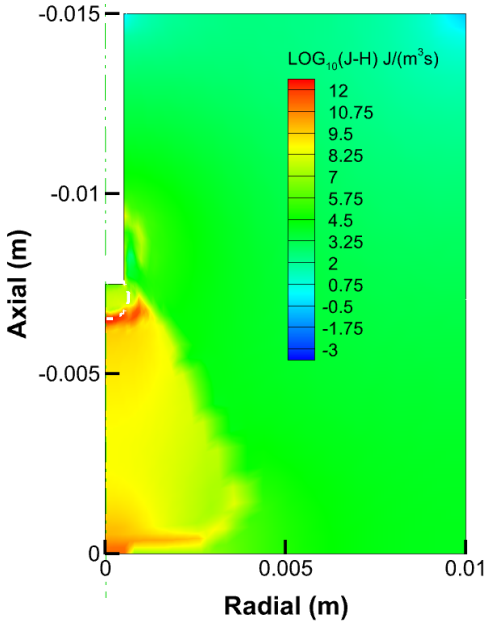

Figure 6. Logarithmic distribution of Joule-heat generation term.

Figure 6 presents the logarithmic distribution of the Joule-heat source term. As seen, there are two high-intensity regions, one near the droplet and another near the bottom, both contributing to the temperature increase. Between these two regions, a less intense generation term (shown in yellow) is observed. Interestingly, the electron-migration distribution presented in Figure 7 closely resembles the Joule-heat term, indicating that this term should not be omitted, as done in [4]. Both terms depend on the current density distribution and electrical conductivity. However, the electron-migration term is also directly influenced by the temperature distribution. This creates a strong coupling between the energy equation and Maxwell's equation, requiring careful numerical setup and the use of small under-relaxation factors.

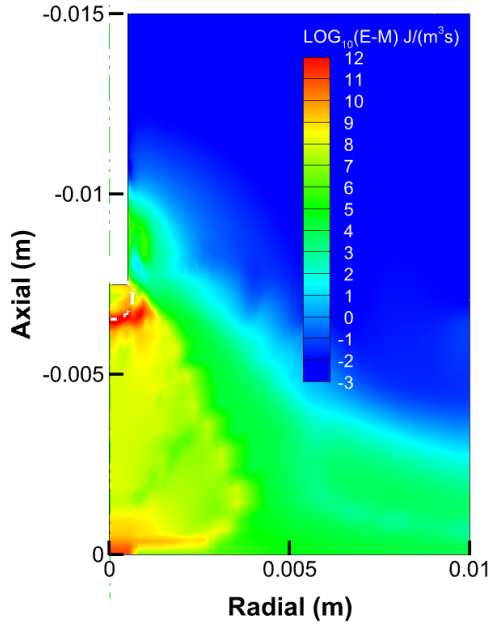

Figure 7. Logarithmic distribution of electron-migration generation term.

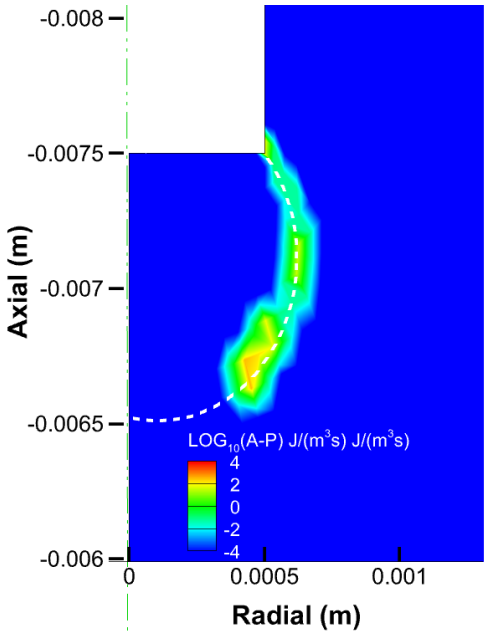

Figure 8. Logarithmic distribution of anode-plasma generation term.

The contribution of anode-plasma heat generation is illustrated in Figure 8. It is seen that, compared to the Joule-heat and electron-migration terms, this term produces significantly lower heat and is confined to the droplet boundary, as expected. Therefore, this term can be omitted from the energy equation for simplicity and to lower the computational costs. Finally, Figure 9 presents the cooling rate of emission (note the negative sign on the plot). Although this term is less intense than the generation terms, it affects a much broader area between the anode (wire tip) and the bottom.

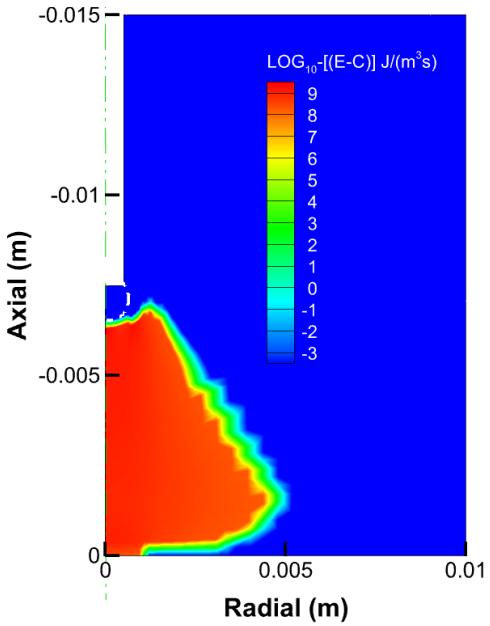

Figure 9. Logarithmic distribution of emission-cooling term.

It should be noted that the emission cooling rate is a linear function of the plasma emission coefficient. The latter is given in the literature and varies with temperature [3,4]. However, to the best of the authors' knowledge, no simple analytical expression has been proposed for it. For our simulations, we developed a Gaussian relation that calculates this coefficient with reasonable accuracy.

$$net\ emission\ coeff. = A \times exp\left[-\frac{(T-B)^2}{2C^2}\right] + D \qquad (10)$$

The coefficients on the right-hand side of Eq. (10) are listed in TABLE I, and a comparison is made in Figure 10.

TABLE I. COEFFICIENTS USED IN EQ. (10).

Coeff.	A	B	C	D
Value	3.47e+09	2.94e+04	6.46e+03	1.11e+07

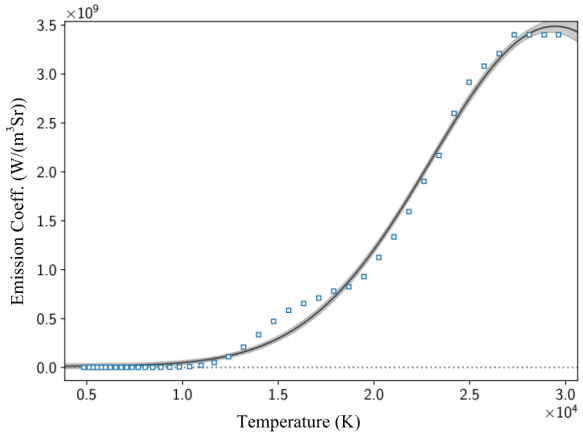

Figure 10. Net emission coefficient, modeled (solid line) vs. experimental data (symbols) [3].

Also, for the electrical conductivity of plasma gas (argon), a new relation is introduced and used in the current study according to the temperature-dependent values provided in the literature [3,4]. The developed relation reads:

$$\sigma = AT^4 + BT^3 + CT^2 + DT + E, \qquad (11)$$

where the coefficients are listed in TABLE II, and a comparison is presented in Figure 11. It should be noted that for temperatures lower than 5000K, a constant value of 0 was used.

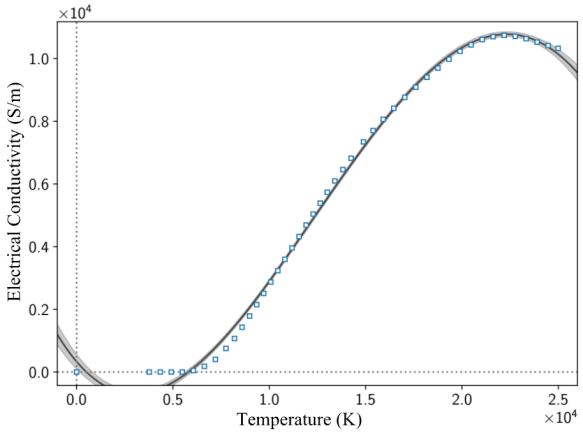

Figure 11. Electrical conductivity, modeled (solid line) vs. experimental data (symbols) [3].

TABLE II. COEFFICIENTS USED IN EQ. (11).

Coeff.	A	B	C	D	E
Value	2.34e-14	-4.37e-09	1.39e-04	-7.22e-01	3.32e+02

IV. CONCLUSIONS

In the current study, the heat distribution in a typical GMA-based WAAM process was numerically investigated. The

existing ambiguities regarding the boundary conditions, initial values, and the contribution of each source term in the energy equation were addressed to assess their significance. The findings indicate that the initial electric potential and temperature play a crucial role in achieving a steady temperature distribution. Also, the electric-migration generation term was shown to be significant in magnitude and should not be omitted. The results of this investigation provide valuable insights for future studies aiming to characterize the WAAM process computationally.

ACKNOWLEDGEMENT

The authors gratefully acknowledge the financial support of the Natural Sciences and Engineering Research Council of Canada (NSERC) under Grant No. [ALLRP 597088].

REFERENCES

[1] 2024, *Wire Arc Additive Manufacturing: Fundamental Sciences and Advances*, Taylor & Francic.

[2] Lowke, J., Kovitya, P., and Schmidt, H., 1992, "Theory of Free-Burning Arc Columns Including the Influence of the Cathode," Journal of Physics D: Applied Physics, **25**(11), p. 1600.

[3] Yujiao, Z., Yinghao, L., Sizhe, N., Hongtao, W., and Ran, Z., 2024, "Multi-Physics Coupling Simulation of GMAW Arc and Droplet Behaviors Based on CFD," Welding in the World, **68**(10), pp. 2589–2610.

[4] Zhao, W., Wei, Y., Tashiro, S., Tanaka, M., and Murphy, A. B., 2023, "Numerical Investigations of Arc Plasma Characteristic Parameters Evolution and Metal Properties in GMAW-Based WAAM of Al Alloy with an Integrated Model," Journal of Manufacturing Processes, **99**, pp. 321–337.

[5] Boselli, M., Colombo, V., Ghedini, E., Gherardi, M., and Sanibondi, P., 2012, "Dynamic Analysis of Droplet Transfer in Gas-Metal Arc Welding: Modelling and Experiments," Plasma Sources Science and Technology, **21**(5), p. 055015.

[6] Murphy, A. B., 2010, "The Effects of Metal Vapour in Arc Welding," Journal of Physics D: Applied Physics, **43**(43), p. 434001.

[7] Rao, Z. H., Hu, J., Liao, S. M., and Tsai, H. L., 2010, "Modeling of the Transport Phenomena in GMAW Using Argon–helium Mixtures. Part I – The Arc," International Journal of Heat and Mass Transfer, **53**(25–26), pp. 5707–5721.

[8] Lowke, J., and Tanaka, M., 2006, "'LTE-Diffusion Approximation'for Arc Calculations," Journal of Physics D: Applied Physics, **39**(16), p. 3634.

[9] Gou, Q., Zhang, Z., Xu, L., Wu, D., Zhang, T., and Liu, H., 2024, "Heat and Mass Transfer Behavior in CMT plus Pulse Arc Manufacturing," International Journal of Mechanical Sciences, **281**, p. 109638.

[10] Liao, H., Zhang, W., Li, X., Pei, K., Lin, S., Tian, J., and Wang, Z., 2022, "Numerical Simulation and Experimental Verification of Droplet Transfer during Local Dry Underwater MIG Welding Process of SUS304," Journal of Materials Research and Technology, **21**, pp. 1960–1973.

[11] Chen, X., Wang, C., Ding, J., Bridgeman, P., and Williams, S., 2022, "A Three-Dimensional Wire-Feeding Model for Heat and Metal Transfer, Fluid Flow, and Bead Shape in Wire Plasma Arc Additive Manufacturing," Journal of Manufacturing Processes, **83**, pp. 300–312.

[12] Zhao, W., Wei, Y., Long, J., Chen, J., Liu, R., and Ou, W., 2021, "Modeling and Simulation of Heat Transfer, Fluid Flow and Geometry Morphology in GMAW-Based Wire Arc Additive Manufacturing," Welding in the World, **65**, pp. 1571–1590.

[13] Hu, Z., Hua, L., Qin, X., Ni, M., Ji, F., and Wu, M., 2021, "Molten Pool Behaviors and Forming Appearance of Robotic GMAW on Complex Surface with Various Welding Positions," Journal of Manufacturing Processes, **64**, pp. 1359–1376.

[14] Zhang, S., Ma, G., Peng, X., and Xiang, Y., 2017, "Numerical Simulation of the Effects of Bypass Current on Droplet Transfer during AZ31B Magnesium Alloy DE-GMAW Process Based on FLUENT," The International Journal of Advanced Manufacturing Technology, **90**, pp. 857–863.

[15] GridPro, 2022, *Program Development Company LLC, Mesh Generation Software.*

[16] Wang, Y., Liu, W., Li, W., Su, X., Zhao, W., Xu, G., and Zhu, J., 2024, "Effects of He-Ar Shielding Gas Compositions on Arc Plasma Physical Properties in Rotating Laser+ GMAW Hybrid Fillet Welding: Numerical Simulation," Optics & Laser Technology, **178**, p. 111231.

[17] Zhao, W., Wei, Y., Xu, G., Liu, X., and Yan, D., 2024, "Numerical Investigation of Arc Characteristics and Metal Properties in ELAMF-Assisted WAAM with Wire Retraction," Vacuum, **230**, p. 113689.

[18] Zong, R., Chen, J., Wu, C., and Lou, D., 2021, "Numerical Analysis of Molten Metal Behavior and Undercut Formation in High-Speed GMAW," Journal of Materials Processing Technology, **297**, p. 117266.